Ultrasonics - Sonochemistry 55 (2019) 279–288

Contents lists available at ScienceDirect

Ultrasonics - Sonochemistry

journal homepage: www.elsevier.com/locate/ultson

Ultrasound exfoliation of graphite in biphasic liquid systems containing ionic liquids: A study on the conditions for obtaining large few-layers graphene

Anna P. Godoy[a], Petra Ecorchard[b], Hynek Beneš[c], Jakub Tolasz[b], Darina Smržová[b], Leandro Seixas[a], Jairo J. Pedrotti[a], Eunezio A.T. de Souza[a], Omar A. El Seoud[d], Ricardo K. Donato[a,*]

[a] MackGraphe (Graphene and Nanomaterials Research Center), Mackenzie Presbyterian University, Rua da Consolação, 930, São Paulo, SP, Brazil
[b] Institute of Inorganic Chemistry of the CAS, v.v.i., 25068 Řež, Czech Republic
[c] Institute of Macromolecular Chemistry of the CAS, v.v.i., Heyrovsky Sq. 2, 16206 Prague 6, Czech Republic
[d] Institute of Chemistry, University of São Paulo, Av. Professor Lineu Prestes, 748, 05508-000 São Paulo, SP, Brazil

ARTICLE INFO

Keywords:
Graphene
Liquid phase exfoliation
Ionic liquids
Biphasic liquid system
Cavitation-based emulsification

ABSTRACT

Herein we describe a successful protocol for graphite exfoliation using a biphasic liquid system (water/dichloromethane, DCM) containing ionic liquids (ILs; 1,3-dibenzylimidazolium benzoate- and 1-naphthoate). The use of (surface active) IL and sonication led to stable DCM/water (O/W) emulsion, which enhanced graphene formation, suppressed its re-aggregation and decreased shear/cavitation damage. The O/W emulsion stabilization by the ILs was studied by dynamic light scattering (DLS), whereas their interaction with the graphene sheets were described by Density Functional Theory (DFT) calculations. Moreover, a comprehensive investigation on cavitation-based exfoliation in the O/W systems was performed to assess the importance of operational parameters, including, the type of ultrasound processor, ultrasound power and insonation, and the influence of the exfoliation medium.

1. Introduction

Recently, the interest in studying two-dimensional (2D) materials has been driven by the development in graphene research. Graphene is a hexagonal lattice of sp^2 hybridized carbon atoms with many unique features that outperform most conventional nanomaterials. This has led to applications in diverse fields, including electronics, optoelectronics and energy storage devices, chemical and biochemical sensors, nanocomposites, etc. [1–4].

The production of monolayer and few-layer defect-free graphene usually requires the use of techniques such as micromechanical exfoliation and Chemical Vapor Deposition (CVD), which present drawbacks such as low yield and non-scalability. Alternatively, the most common approach reported in the literature involves an aggressive graphite oxidation followed by exfoliation in water (Hummer's method). The resulting product is graphene oxide (GO), which, upon reduction, yields reduced graphene oxide (rGO) [5–7]. However, this method also presents limitations, *e.g.*, demands the use of toxic reactants, is highly exothermic and leads to structural defects. The development of more scalable, reliable, non-oxidative, safe and sustainable methods became a necessity as this field progressed [8–10]. The preparation of rGO using environmentally friendly reducing agents of GO such as extract of *Ganoderma lucidum* mushroom [11], vitamin C [12], green tea [13] and bacteria [14] was reported. However, that did not solve the oxidative step, which is the most aggressive and residue producing.

Graphite liquid phase exfoliation (LPE) is regarded as a promising scalable route of graphene production. It is based on suspension of graphite in a suitable solvent and application of energy, *e.g.*, ultrasonic [15] or shear force mixing [16], which results in graphite delamination into individual sheets. Previous works reported graphene production with high yields and scalability using organic solvents and/or surfactant solutions as LPE media [17–19]. The solvent properties play a crucial role, since the solvent surface tension needs to match that of graphene ($\sim 40\ mJ.m^2$) [20].

Considering the case of aromatic solvents, the graphene-solvent noncovalent π-π interactions are important since they do not alter the graphene's structural and electronic properties. There are two types of

* Corresponding author.
E-mail address: ricardo.donato@mackenzie.br (R.K. Donato).

https://doi.org/10.1016/j.ultsonch.2019.01.016
Received 12 September 2018; Received in revised form 27 December 2018; Accepted 14 January 2019
Available online 16 January 2019
1350-4177/

graphene-aromatic solvent π-π interactions; face-to-face stacking between the electron-rich regions, and edge-to-face (C-H—π) among electron-poor regions. Moreover, the geometry (namely planarity), size and presence of substituents also influence the graphene's final structure and electronic properties. Considering a pristine graphene monolayer, it comprises of extended aromatic system with almost planar geometry. Consequently, it interacts better with small aromatics molecules since they slowly penetrate in between graphene layers and promote delamination, *e.g.*, during sonication [21]. Additionally, the use of aromatic solvents with hydrophilic or hydrophobic substituents assist the graphene sheets' stabilization in water or organic solvents, respectively [22–23].

Within this context, the application of ionic liquids (ILs) have shown promising results and interesting perspectives for graphite exfoliation because of their thermal and chemical stability, good electrical and thermal conductivities, as well as stabilization and morphology control properties [24–29], among other properties. Imidazole-based ILs provide strong π-π interaction between the imidazolium cation and graphene, while electrostatic repulsion prevents layer re-aggregation [30].

Pioneer works demonstrated that, using 1-butyl-3-methylimidazolium bis(trifluoromethanesulfonyl) imide ([C_4MIm(NTf_2)]) as solvent and tip ultrasonication produced few layers graphene with concentrations up to 0.95 mg. mL^{-1} [31], whereas grinding graphite flakes within 1-n-hexyl-3-methylimidazolium hexafluorophosphate ([C_6MIm(PF_6)]) in a mortar before sonication produced 5.33 mg. mL^{-1} of graphene [32]. Moreover, high quality graphene sheets and nanodots from natural graphite exfoliation with 1-n-butyl-3-methylimidazolium hexafluorophosphate ([C_4MIm(PF_6)]) were produced by sequential mechanical grinding and sonication [33]. In an approach developed by Matsumoto *et al.*, single layer graphene was obtained by microwave irradiation-assisted LPE of graphite in two ILs with oligomeric cations and PF_6 anion. The HF molecules, produced by PF_6 hydrolysis, intercalated among graphite sheets, helped exfoliation, while maintained the structural integrity of the produced graphene [34]. Moreover, the influence of aromatic substituents in imidazolium based ILs for graphene stabilization was also reported [35].

The role of ultrasonication in graphene production is to overcome the van der Waals forces that bind graphite layers. Ultrasound waves comprise compression and rarefaction cycles. During the latter, the negative acoustic pressure is sufficiently large to rupture the liquid creating stable or transient micro bubbles, responsible for cavitation. These cavitation bubbles grow fast and collapse violently with an instantaneous and intense local heating (up to 5000 K), high pressure (up to 20 MPa) and fast heating/ cooling rates (10^{10} $K.s^{-1}$) [36–39]. Ultrasound application to biphasic water-(immiscible) organic solvent leads to emulsification by two mechanisms: (i) the ultrasound waves at the oil/water (O/W) interface leads to inclusion of oil droplets into water; (ii) bubble collapse during cavitation causes highly localized turbulence and break up the dispersed oil phase droplets into sub-micron size [40–41]. The presence of surfactants, including (surface active) ILs [42], in this media decreases the droplets coalescence, hence increases the O/W emulsion stability [43].

Using this approach, we developed a one-step protocol for the production of few layers graphene. It was based on the exfoliation of an inexpensive (untreated) graphite ore in biphasic liquid systems, consisting of water/dichloromethane or water/octanol, also containing 1-butyl-3-methylimidazolium bis(trifluoromethanesulfonyl) imide ([C_4MIm(NTf_2)]), using a closed-vessel ultrasound reactor (2 kW) pressurized to 5 bars. In this system, the exfoliated graphene sheets were confined at the water-organic solvent interphase, while the pristine (bulky) material and mineral residues remained in the aqueous phase [44].

Here we present a comprehensive study of graphite LPE in biphasic liquid system (dichloromethane/water; DCM/W) in the presence of the ILs 1, 3- dibenzylimidazolium benzoate, [$(Bnz)_2$Im(Benz)], and 1,3-dibenzylimidazolium 1-naphtoate, [$(Bnz)_2$Im(Naph)]. We analysed the effects of: type of cavitation processor; ultrasound power; insonation, and the biphasic liquid system composition. The results of DFT calculations gave insight into the ILs role at the liquid-graphene interphase. Finally, the produced graphene's structural quality and morphology was characterized and compared to other previously described methods.

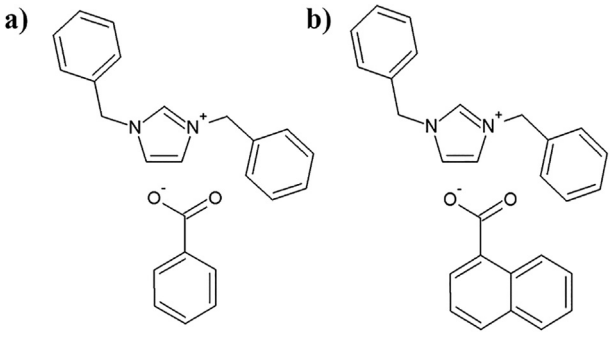

Fig. 1. Molecular structures of the ILs used in the present work: (a) [$(Bnz)_2$Im(Benz)] and (b) [$(Bnz)_2$Im(Naph)].

2. Experimental part

2.1. Materials

The graphite flakes used were purchased from Sigma Aldrich (99.9% pure). All chemicals were purchased from Alfa Aesar, Carlo Erba, Sigma Aldrich and Synth (São Paulo) and were purified, where required, as recommended elsewhere [45].

2.2. Ionic liquid synthesis

The ILs [$(Bnz)_2$ Im(Benz)] and [$(Bnz)_2$Im(Naph)] (Fig. 1) were synthesized as follows. For obtaining 0.1 mol of IL, firstly, a sodium ethoxide solution was prepared dissolving 6.8 g of metallic sodium (99.8% Alfa Aesar) in 200 mL of isopropanol. After dissolution, 20 g of imidazole (99.9% Alpha Aesar) was added and it was kept under reflux during 2 h.

Isopropanol was removed and the solid was mixed with 50 mL of acetonitrile (99.5% Synth), followed by addition of 180 g benzyl chloride (99% Sigma Aldrich, 0.2 mol) in 25 mL of acetonitrile (99.5% Synth) at room temperature. The mixture was kept under reflux and microwave irradiation (Discover DU-8316, CEM, 100 W) during 4 h. After acetonitrile distillation, the product was washed with 20 mL of cold ethyl acetate (98.5% Synth) for three times and dried. The exchange between chloride and hydroxyl anions was made through an ionic exchange resin (Purolite SGA-550-OH; OH form). The product was neutralized with benzoic acid (Carlo Erba) or 1-Naphthoic acid (98% Sigma Aldrich) to obtain, respectively, [$(Bnz)_2$Im(Benz)] and [$(Bnz)_2$Im(Naph)], which were dried in vacuum oven. The purity of ILs was confirmed by ^{1}H NMR and Raman spectroscopy (Supporting information, Figs. S1, S2 and S4).

2.3. Exfoliation process in ultrasound bath

Graphite flakes (0.01 g) and [$(Bnz)_2$ Im(Benz)] or [$(Bnz)_2$ Im(Naph)] (0.1 g) were added to a glass vessel containing 20 mL of the biphasic solvent system composed of deionized water (MilliQ) (95%) and dichloromethane (DCM) (5%). The vessel was closed and sonicated into an ultrasound bath (Elmasonic 30H, 320 W, amplitude of 100% and 37 Hz) at 10° C for 5 h. O/W emulsion samples were withdrawn every 1 h for time dependent graphene characterization.

2.4. Exfoliation process in ultrasound probe

Two types of ultrasound probe processors were used to sonicate the graphite in an open system: i) a 2 mm diameter titanium alloy microtip probe (SONICS Vibra Cell 130 W and 20 Hz) operated at 90% amplitude (117 W nominal power); and ii) a 14 mm diameter titanium sonotrode (UP400S Hielscher, 400 W and 24 Hz) operating at 70% amplitude (280 W nominal power). The sonication experiment was carried out as given in 2.3, except for duration (40 min) and sampling time (every 10 min).

2.5. Biphasic liquid system characterization

2.5.1. Dynamic light scattering (DLS)

We employed DLS to evaluate emulsion droplets hydrodynamic diameters and their stability in presence and absence of [$(Bnz)_2$Im(Benz)]. Two sets of biphasic systems were investigated, with and without [$(Bnz)_2$Im(Benz)], in four H_2O/DCM volume ratios; 95/5, 90/10, 75/25 and 50/50. The solvent mixtures were sonicated with a ultrasound probe (UP 400S Hielscher, 400 W and 24 Hz) for 10 min at 10 °C. Immediately after sonication, the emulsions were transferred to a quartz cuvette and the medium light scattering measured after 2 min equilibration time with Litesizer 500 Anton Paar equipment (40 mW He/Ne laser, 658 nm, 20 min acquisition time).

The droplet hydrodynamic diameter was calculated by the Stokes-Einstein equation for hard spheres (Eq. (1)):

$$D_h = K_B T / 3\pi \eta D_T \quad (1)$$

where D_h is the hydrodynamic diameter; D_T is the diffusion coefficient; k_B is the Boltzmann constant (1.3806×10^{-23} m^2 kg s^{-2} K^{-1}); T is temperature (K) and η is the dynamic viscosity (m^2 s^{-1}).

2.5.2. Optical microscopy

A droplet of 95/5 H_2O/DCM emulsion containing [$(Bnz)_2$Im(Benz)] (prepared as given in 2.5.1) was sandwiched between two microscope glass slides and observed with an Olympus BMX51 reflected light optical microscope. The images were examined using 40x magnification and dark field mode (S3).

2.6. Materials modelling and simulation

Interactions between IL and graphene were computationally modelled by density functional theory (DFT) calculations implemented by SIESTA code [46–48]. To calculate electronic densities we used double-ζ basis set with polarization orbital (DZP), energy cutoff of 600 Ry, GGA-PBE exchange-correlation functional [49] and Troullier-Martins pseudopotential [50]. Unit cells of 4.28 nm^2 were simulated with periodic boundary conditions and k-points sampling in a 2 x 2 x 1 Monkhorst-Pack method [51]. The relaxed IL structures were calculated using maximum forces of 0.04 eV $Å^{-1}$ and van der Waals forces corrections based on Grimme's approach (D2) [52]. To complement the relaxed IL geometries and electronic structure calculations, we performed first-principles molecular dynamics (FPMD) simulations within NVT ensemble, with Nosé thermostat at 298 K. The FPMD were performed with total time of 10.0 ps, with 1.0 fs time step. In these FPMD simulation, IL is represented by three cations and three anions per unit cell. To speed up the FPMD simulation, we use single-ζ basis, lower energy cut-off of 150 Ry and Γ-point calculations.

2.7. Graphene characterization

2.7.1. Raman spectroscopy

A Confocal Microscope Spectrometer (Witec Alpha 300R) using 50 and 100x objective lens, grading of 600 g/mm and 532 nm excitation laser was employed to firstly characterize the exfoliated graphite. A silicon oxide substrate was used to calibrate the spectrometer.

The samples were prepared by dropping 10 μL of the emulsion obtained onto silicon oxide wafer substrates. After solvent evaporation, the IL excess was washed by soaking the substrates in ethanol overnight, followed by drying under vacuum during 1 h. This procedure was performed due to the IL's intrinsic tendency to produce luminescence, overlapping the Raman signal. The Raman results represent an average of 25 Raman single spectra for each sample.

2.7.2. Scanning electron microscopy (SEM)

The samples for SEM characterization were prepared by producing a DCM droplet onto a copper grid (200 mesh) followed by dropping an aliquot of 4 μL of the obtained emulsion, which was further dried under vacuum for 1 h. SEM images were recorded using a JEOL JSM 7800F (30 kV) with STEM mode and 10 000 to 30 000× of magnification.

2.7.3. Atomic force microscopy (AFM)

The AFM characterization was carried out using a Bruker Icon Dimension Microscope in ScanAsyst-air contact mode. A biphasic liquid system was prepared on a mica substrate by adding a small amount of both H_2O and DCM. The samples were then collected directly from biphasic liquid exfoliation media, diluted with DCM (200×), added over the pre-treated mica and spread by rotation (spin coating), followed by drying under vacuum for 1 h.

2.7.4. Transmission electron microscopy (TEM)

The samples for TEM structural and morphological analyses were prepared by the following procedure: after sonication, the biphasic systems were diluted with a mixture of H_2O and DCM (1:200). The diluted samples were dropped (4 μL) directly onto a lacey carbon coated copper grid. The sampled grid was dried under vacuum for 4 h at 80 °C. Samples were measured using a Talos F200X HRTEM (FEI) electron microscope at 120 kV.

3. Results and discussion

Biphasic solvent systems have been reported as effective exfoliation medium for 2D materials, which allow self-assembly at the liquid-liquid interface by using the interfacial energy between the immiscible phases [53–56]. Considering the graphene production, graphite could be successfully exfoliated in H_2O/chloroform, H_2O /n-heptane, H_2O/DCM and H_2O/n-octanol biphasic systems. Moreover, based on the liquids' densities these systems allowed choosing where the exfoliated graphite would be preferentially located [57]. The use of ILs for stabilizing these systems was also described [44]. However, information about the relevance of the following experimental variables is missing: i) the ultrasound source type and power, ii) the effect of different biphasic system phase ratios, and iii) the molecular structure of the IL. These aspects are addressed below.

3.1. Biphasic systems stability and structure

Using DLS, different biphasic systems, with and without IL, were investigated, as well as their stability after ultrasound emulsification. The aspect of interest was the evolution of droplet hydrodynamic diameter with time because this bears on emulsion stability, hence the efficiency of exfoliation.

The DLS measurements were performed on emulsions of four different H_2O/DCM volume ratios 95/5, 90/10, 75/25 and 50/50, in the presence (I) and absence (II) of the IL [$(Bnz)_2$Im(Benz)]. The evolution of the droplets hydrodynamic diameters as a function of time after sonication is displayed in Fig. 2.

The systems without IL (Fig. 2 I) showed initial hydrodynamic diameters between 0.3 and 5 μm (systems with 95/5 and 50/50 vol ratios, respectively). After approximately 8 min, an increase in droplet diameter was noted for 75/25 and 50/50 (curves 2c and d in Fig. 2 I) biphasic system, followed by a drastic reduction, indicating droplet

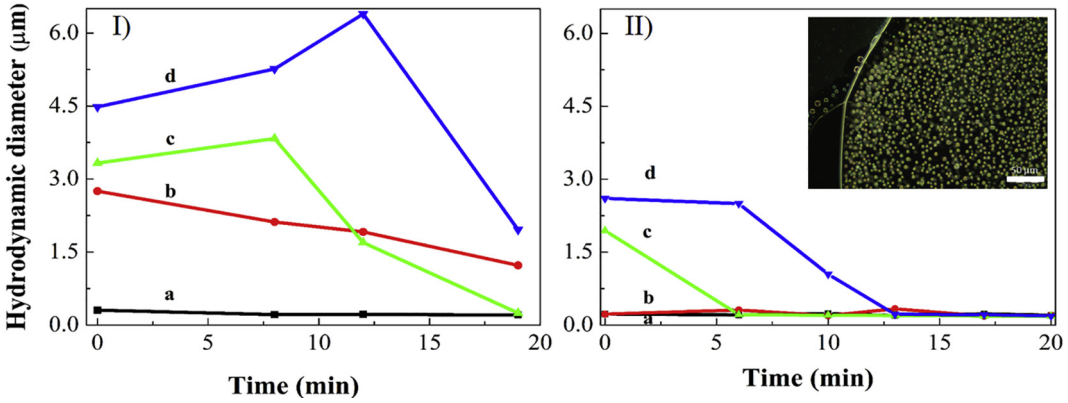

Fig. 2. Biphasic liquid systems in (I) absence and (II) presence of IL, with H_2O/ DCM volume ratios of (a) 95/5, (b) 90/10, (c) 75/25 and (d) 50/50. The insert presents a dark field polarized light optical microscopy image of the H_2O/ DCM = 95/5 system in the presence of IL (scale bar = 50 μm).

coalescence followed by macrophase separation. The 95/5 (a) and 90/10 (b) biphasic systems presented only a very small diameter variation during all the measurement duration.

In contrast, the systems containing IL presented initial diameters between 0.2 and 2.6 μm (systems with 95/5 and 50/50 vol ratios, respectively), values almost twice smaller than for systems without IL when considering systems 75/25 and 50/50 (curves c and d in Fig. 2 II). The latter exhibited coalescence followed by phase separation after less than 10 min. On the other hand, the 95/5 biphasic system, both without and with IL (Supporting Information Fig. S10), formed a stable emulsion with droplet hydrodynamic diameter of less than 1 μm, and represents, therefore, the most suitable for graphite exfoliation.

3.2. DFT simulations of graphene-IL interactions

The IL-graphene interactions present an important role in the LPE process efficiency [31–35]. However, the ILs interaction capacity is always strongly associated with their molecular structure that determines its bonding to the graphene surface. The relevance of the latter interactions was probed by DFT calculations. As shown below, the results of these calculations were employed to choose $(Bnz)_2Im(Benz)$ as a more promising candidate for graphite LPE.

The influence of benzyl substituents in the imidazolium cation on graphite exfoliation was already reported. It was demonstrated that the binding energy between the 1,3-dibenzyl imidazolium cation ($[(Bnz)_2Im]^+$) and graphene is -30.6 kcal mol^{-1} with a binding distance of 3.20 Å [35]. However, we obtained for the same cation the value of –33.41 kcal mol^{-1} and observed that the highest contribution results from the interaction between the imidazolium ring and the graphene surface, instead of the benzene rings (Fig. 3a). This means that the imidazolium ring has a more intimate binding (3.23 Å) with graphene than the benzene rings, i.e., the former ring is more important to stabilize mono/few layers graphene. Moreover, the bis(trifluoromethylsulfonyl)imide anion (NTf_2^-), often used as IL anion due to its good affinity with many 2D materials, presented a binding energy of -11.7 kcal mol^{-1} [35]. Both anions used in this work presented more favorable binding energy, -13.8 kcal mol^{-1} for benzoate $(Benz)^-$, and -13.01 kcal mol^{-1} for 1-naphthoate $(Naph)^-$.

The efficiency of the present ILs is presumably a consequence of their more planar structures that allow a closer binding with the graphene surface (Fig. 3b and c). However, increasing the number of aromatic rings in the anion did not lead to stronger interactions, as $(Benz)^-$ (one benzene ring) has a higher binding energy to graphene than $(Naph)^-$ (two benzene rings), presumably due to the higher molecular rigidity in the $(Naph)^-$ (Fig. 3b and c).

FPMD simulations of the IL presenting the best interactions to graphene, $(Bnz)_2Im(Benz)$, were performed considering 3 IL ion pairs and a graphene sheet. These simulations consisted in evaluating the behaviour of IL ion pairs randomly spread near a graphene sheet and by following the time evolution of conformations from thermal effects. Interestingly, the tendency of $(Bnz)_2Im(Benz)$ to interact with graphene is so strong that it overcomes its own intramolecular interactions and self-assembles in an organized fashion onto the graphene sheet (Fig. 3d and e; SI Video 1 and Video 2). *In summary*, DFT simulations indicated that $(Bnz)_2Im(Benz)$ is probably a better candidate for graphite LPE. This expectation was verified experimentally, as will be further demonstrated.

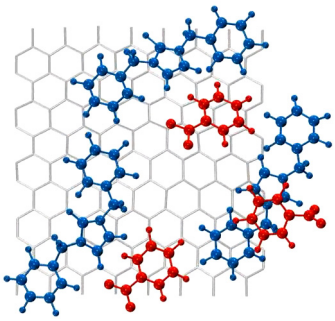

Video 1.

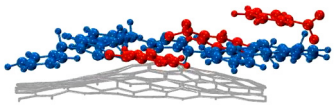

Video 2.

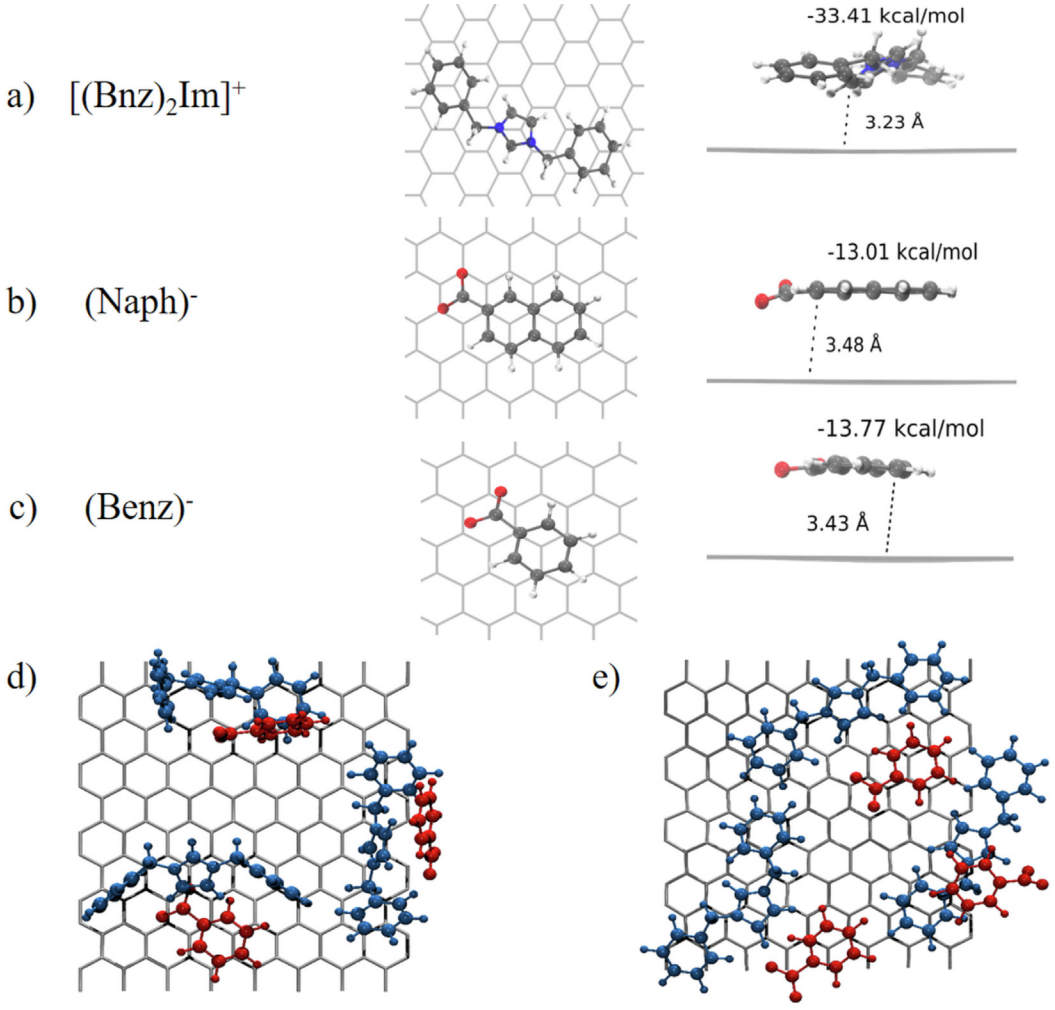

Fig. 3. Top and side view of the interactions of the IL cation $[(Bnz)_2Im]^+$ (a), and anions $(Benz)^-$ (b) and $(Naph)^-$ (c) with a graphene sheet, and the corresponding binding energies and distances calculated by DFT. Initial (d) and final (e) snapshots of the FPMD simulation of the $[(Bnz)_2Im]^+$ $(Benz)^-$ ion pairs self-assembly onto the graphene sheet surface. Molecular colour guideline: (a-c) carbon atoms (grey), nitrogen atoms (blue), oxygen atoms (red) and hydrogen atoms (white); (d) and (e) graphene sheet (grey), $[(Bnz)_2Im]^+$ (blue) and $(Benz)^-$ (red). The FPMD simulations video is shown in the supporting information (SI videos). (For interpretation of the references to colour in this figure legend, the reader is referred to the web version of this article.)

3.3. Graphite flakes exfoliation

The characteristics of produced graphene can be readily identified in terms of quality, structural integrity and level of exfoliation using Raman Spectroscopy, SEM, TEM, AFM and XRD techniques. Herein, these techniques were employed to evaluate the graphene obtained by graphite LPE under different condition. In particular, we wanted to assess the relevance of parameters such as the type of cavitation processor, the influence of ultrasound power and insonation, and the influence of different exfoliation media.

Firstly, the importance of IL presence in the biphasic liquid system to exfoliate the graphite using bath and ultrasound probe (117 W) was examined by Raman Spectroscopy (Fig. 4). The presence of IL enhances the LPE efficiency according to 2D bands (Fig. 4 I). The shift and increase in the 2D bands intensities for both ultrasound types (bath 320 W and probe 117 W) evidenced the formation of few-layered material. This was especially observed for the ultrasound bath process in the presence of $[(Bnz)_2Im(Benz)]$, where the 2D band was even more intense than the G band, indicating a considerable presence of graphene with less than three layers [53]. These results were confirmed by XRD results, showing an almost complete disappearance of the (0 0 2) peak referring to the graphite interlayer distance (Supporting Information, Fig S9). Moreover, only an insignificant increase in the Raman D bands was observed, indicating the crystalline phase preservation. The same preservation was noted for the ultrasound probe application (Fig. 4 II).

Raman Spectroscopy was also employed to evaluate the quality and integrity of produced graphene when exfoliated in the presence of the different ILs, as well as different power application for ultrasound probe (Fig. 5). Important parameters obtained by Raman spectra are the ratio between D and G band intensities (I_D/I_G) indicating the structural integrity [53], as well as the ratio between 2D and G band intensities (I_{2D}/I_G), indicating the graphite's degree of exfoliation.

Graphite LPE using ultrasound bath with the biphasic system containing $[(Bnz)_2Im(Benz)]$ led only to a small increase of the D band and the presence of a very intense 2D band (Fig. 5 I). The I_D/I_G ratio was 0.25, whereas the I_{2D}/I_G was 1.07. The latter value is generally related to very few graphene layers (less than3) [58]. The performance of $[(Bnz)_2Im(Naph)]$ was slightly less effective, showing I_D/I_G and I_{2D}/I_G ratios of 0.43 and 0.46, respectively. Considering the 2D bands, the ultrasound bath led to more effective exfoliation than probe sonication. It is worth noting that the systems were applied under different conditions for the two different types of ultrasound processors. The ultrasound bath allowed using closed systems (closed reaction vessels), while the ultrasound probe used open systems (open vessels for probe access). Although all the systems were cooled to a temperature (10 °C) much lower than the boiling point of DCM (39.6 °C), these differences

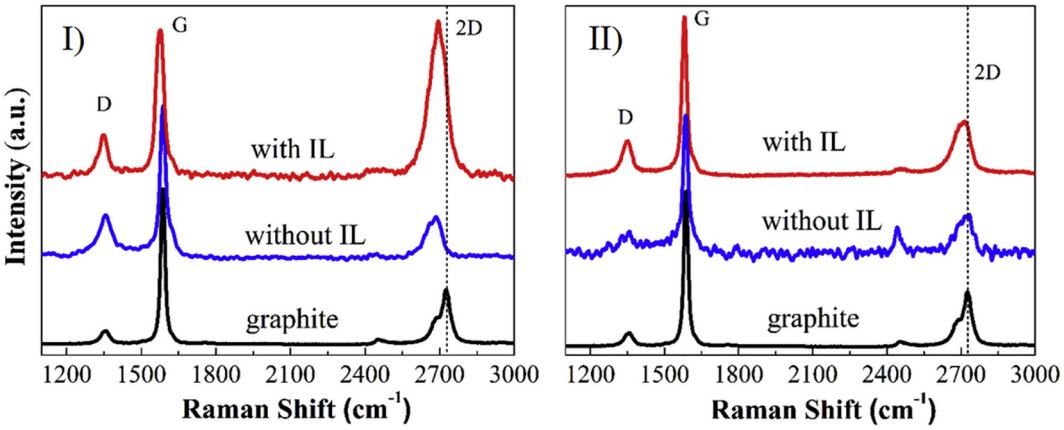

Fig. 4. Raman spectra of graphite exfoliated in biphasic liquid system in the presence and absence of [$(Bnz)_2$Im(Benz)] using bath (320 W) (I) and probe (117 W) (II) ultrasound processors.

in experimental set-ups could affect the solvents ratio during the cavitation process.

Further observations, using the [$(Bnz)_2$Im(Benz)], showed that 30 min sonication using a 117 W ultrasound probe produced graphene with a slightly more intense D band (1347 cm^{-1}), that can be attributed mostly to edge defects, but already with few layers (2D band shift to 2708 cm^{-1}) (Fig. 5 II). Interestingly, the D band intensity (1358 cm^{-1}) did not increase using a 280 W probe. However, the 2D band (2725 cm^{-1}) was more characteristic of a graphitic material [58]. This highlights the possible DCM evaporation with power increase, altering the biphasic liquid system composition and decreasing the exfoliation efficiency. The I_D/I_G and I_{2D}/I_G ratios were of 0.21 and 0.42, respectively, for the 117 W ultrasound probe and 0.10 and 0.33, respectively, for the 280 W ultrasound probe. Since the increase in processor power means more energy released into the system and heating, more bubbles are generated by solvent evaporation and the material's delamination becomes less effective, explaining the I_{2D}/I_G decrease.

The I_D/I_G and I_{2D}/I_G ratios obtained for the exfoliated graphene in biphasic system containing [$(Bnz)_2$Im(Benz)] and [$(Bnz)_2$Im(Naph)] under different ultrasound processors are compared in Table 1. The biphasic liquid system containing [$(Bnz)_2$Im(Benz)] was more effective than using [$(Bnz)_2$Im(Naph)]. The best condition to produce few-layer graphene (I_{2D}/I_G = 1.07) was reached when the ultrasound bath processor was applied. This approach only slightly increased the number of defects (I_D/I_G = 0.25) in comparison to the ultrasound probe, owing to the longer insonation. In the case of ultrasound probe, the 117 W was better than 280 W in terms of exfoliation efficiency (I_{2D}/I_G = 0.43) but led to the production of more defective graphene sheets.

Table 1
I_D/I_G and I_{2D}/I_G ratios obtained for the exfoliated graphite in biphasic liquid system containing [$(Bnz)_2$Im(Benz)] and [$(Bnz)_2$Im(Naph)] under different ultrasound processors.

Material	Ultrasound type/Power	Time	[$(Bnz)_2$Im(Benz)]		[$(Bnz)_2$Im(Naph)]	
			I_D/I_G	I_{2D}/I_G	I_D/I_G	I_{2D}/I_G
Graphite	Bath/ 320 W	5 h	0.25	1.07	0.44	0.47
Graphite	Probe/ 117 W	30 min	0.21	0.43	0.21	0.31
Graphite	Probe/ 280 W	30 min	0.10	0.33	-	-

The Raman results confirmed the conclusions of the DFT simulations that [$(Bnz)_2$Im(Benz)] had stronger interaction with graphene than [$(Bnz)_2$Im(Naph)]. Therefore, the detailed microscopic characterization was only performed on the graphene sheets produced via LPE with [$(Bnz)_2$Im(Benz)].

The structure of exfoliated graphene was further evaluated by AFM (Fig. 6) and SEM/TEM (Fig. 7 and Supporting Information Figs. S6, S7 and S8). It is worth noting that the micrographs are used to demonstrate the thinnest species that are obtained in large amounts for each system. For reaching a reliable conclusion on the range of layers of the exfoliated species, these micrographs were compared to the Raman results and XRD. When ultrasound bath was used in the absence of IL, the graphite exfoliation occurred with efficiency and very thin material was obtained (close to monolayers). The material obtained, however, was bent and highly damaged (Fig. 6a), leading to random electron diffraction (ED) pattern (Fig. 7a) or even presence of amorphous carbon

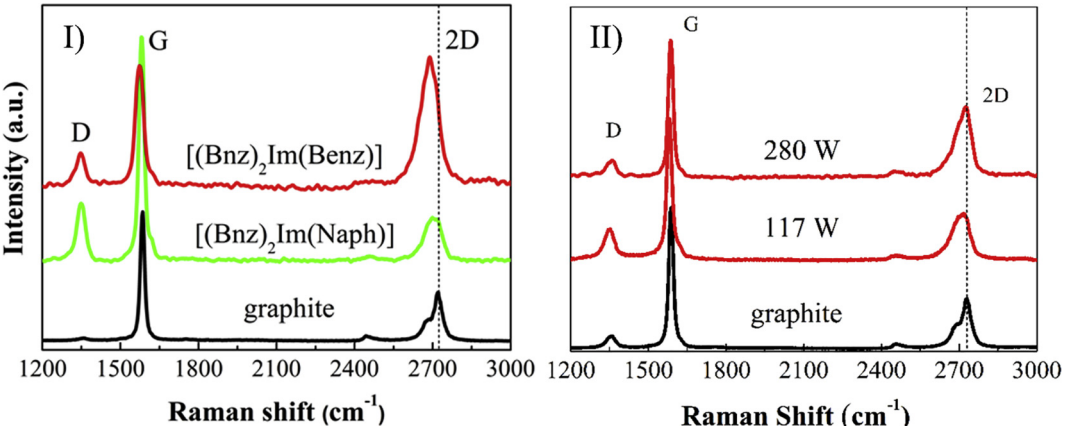

Fig. 5. Raman spectra of graphite exfoliated in biphasic liquid systems containing: [$(Bnz)_2$Im(Benz)] and [$(Bnz)_2$Im(Naph)] (I) by ultrasound bath for 5 h; and [$(Bnz)_2$Im(Benz)] comparing the influence of ultrasound probe power (II). Black dashed line over pristine graphite shows the 2D band position.

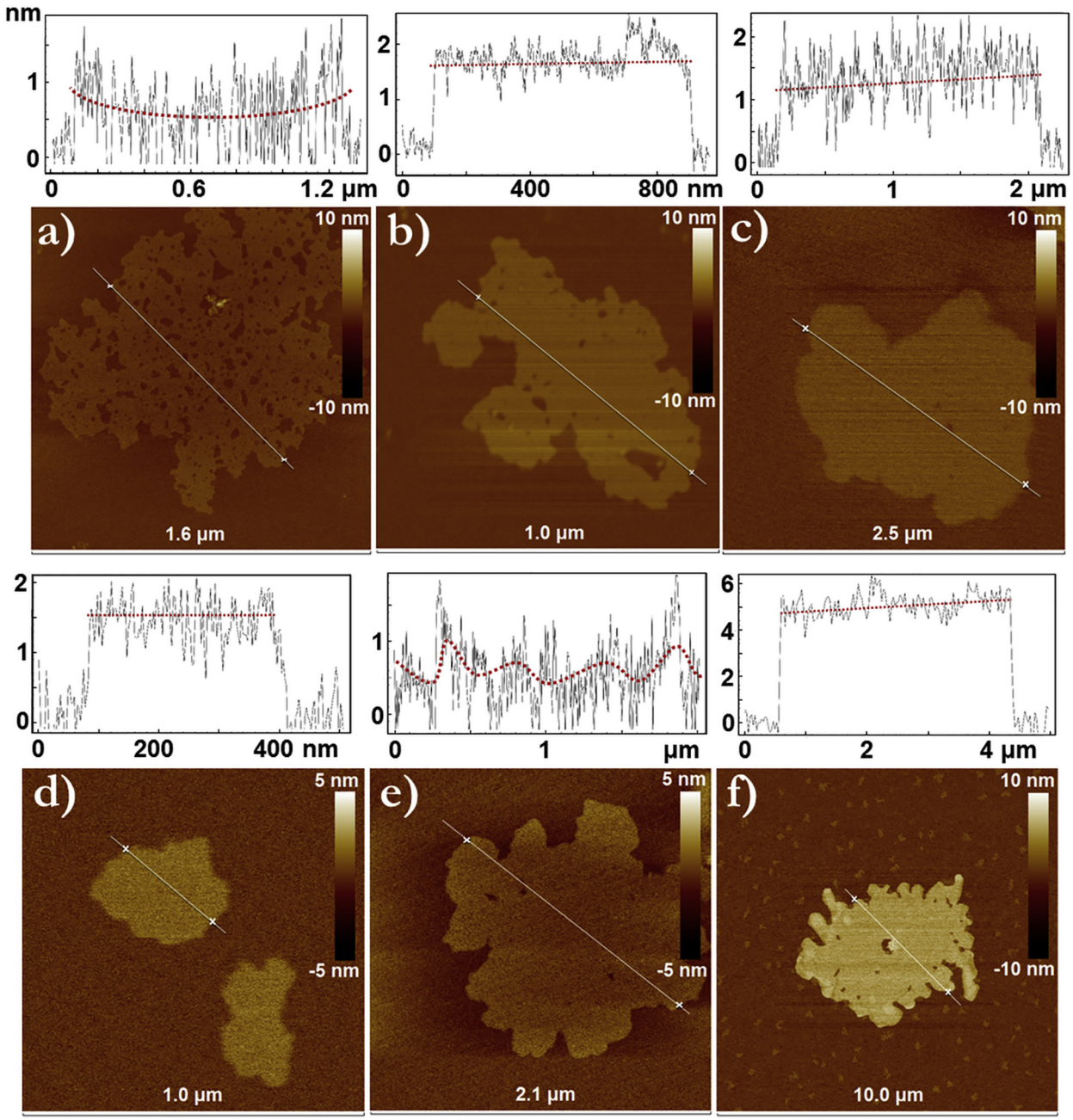

Fig. 6. AFM images, including the topology profiles of exfoliated graphite in biphasic liquid systems; (a) in the absence of IL after 5 h of ultrasound bath; (b) in the presence of $[(Bnz)_2Im(Benz)]$ after 1 h and (c) 5 h of ultrasound bath; (d) in the absence of IL and (e) in the presence of $[(Bnz)_2Im(Benz)]$ after 30 min of 117 W ultrasound probe; (f) in the presence of $[(Bnz)_2Im(Benz)]$ after 30 min of 280 W ultrasound probe. The red dotted lines were drawn as guide for the eye. (For interpretation of the references to colour in this figure legend, the reader is referred to the web version of this article.)

evidenced by the lack of electron diffraction (Fig. S6a).

Applying $[(Bnz)_2Im(Benz)]$ for the same process resulted in large low-defect sheets, in which the thickness was dependent on the sonication time. After 1 h of sonication in ultrasound bath was applied thicker sheets were obtained (Fig. 6b and S6b), whereas 5 h of ultrasound produced a very well exfoliated and with good structural quality graphene (Fig. 6c, S6c and 7b). Moreover, SEM images (Fig. 7c) indicated superficial bubbles and grey spots revealing the IL presence on the graphene surface. When the 117 W ultrasound probe was used, the IL preserving effect on the produced graphene sheets could also be observed (Fig. S7b), although after 30 min sonication some damage to the structural integrity was evidenced (Fig. 6e, 7e and S7c). On the other hand, the same 30 min of 117 W probe sonication, applied in the absence of IL, produced smaller (Fig. 6d) and more damaged sheets (7d and S7d). However, even in the presence of IL, when the ultrasound power was increased, a decrease in exfoliation efficiency was observed, represented by thicker graphene sheets (Figs. 6f and 7f), although keeping a large lateral size and a heterogeneous structural integrity (Fig. 7f and S8).

In summary, the IL-assisted sonication produced graphene with larger lateral dimensions and fewer defects in comparison with the system without IL and the sheet thickness was dependent on the insonation. Especially the reduction of lateral dimension is intimately related to breakage provided by the long exposure to cavitation, but the presence of IL seems to help dissipating the intensive cavitation energy.

Comparing our protocol with the literature data (Table 2), the present work showed that the use of biphasic liquid system improved the process, avoiding the centrifugation step as it allows the separation

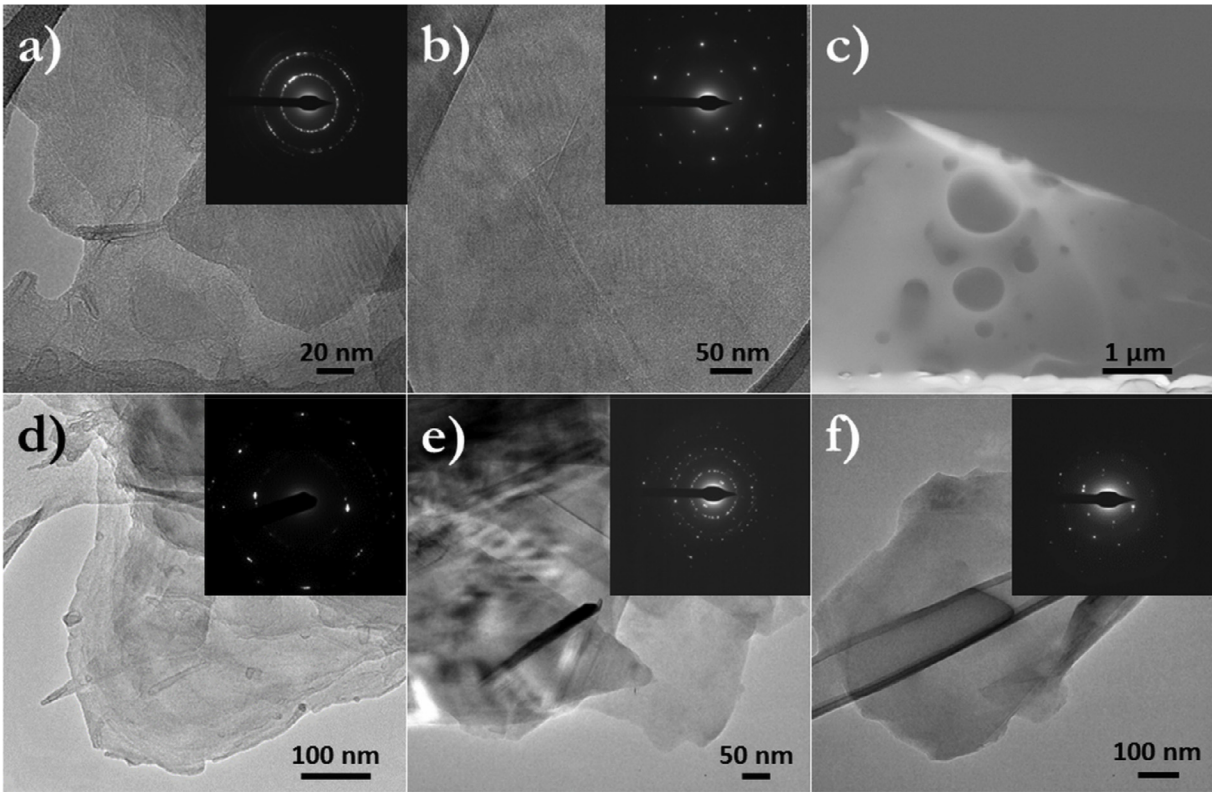

Fig. 7. Electron microscopy images of exfoliated graphite in biphasic liquid systems: TEM after 320 W ultrasound bath for 5 h in the absence of IL (a); TEM (b) and SEM (negative image); c) after 320 W ultrasound bath for 5 h with [$(Bnz)_2$Im(Benz)]; TEM after 117 W ultrasound probe for 30 min without (d) and with [$(Bnz)_2$Im(Benz)] (e); and TEM after 280 W ultrasound probe for 30 min with [$(Bnz)_2$Im(Benz)] (f). The figure inserts are the correlated electron diffraction patterns from TEM.

of produced graphene from the residual graphite. The mild conditions employed prevent edge breakage by intense sonication, as revealed by the low I_D/I_G ratios.

The number of graphene layers can be estimated comparing the flake thickness as obtained by AFM with Raman spectroscopy parameters related to 2D band as the number of Lorentzian curves fitted by deconvolution method, their positions and intensities. Although the use of these parameters is arbitrary, their combination with other techniques is helpful to interpret the extent of the material's exfoliation, even if not with exact accuracy. Moreover, for samples with large structural disorder the Full Width at Half Maximum (FWHM) value should be considered. This is a measure of structural disorder, producing a quantitative guide to distinguish up to 5 layers [59,61]. According to literature, the monolayer graphene has an individual Lorentzian component, while bilayer graphene presents four. In terms of position, the more the 2D band position is blue-shifting from 2700 cm^{-1} (bulk graphite's 2D band position), the more the material is exfoliated. For monolayer graphene, the 2D band is positioned around 2690 cm^{-1} [58–61].

The number of layers for the resulting graphite exfoliated into biphasic liquid system in the presence of [$(Bnz)_2$Im(Benz)], presented in (Table 2), was based on the approach described above. As depicted in Fig. S5a, the 2D band deconvolution of the exfoliated graphite obtained with ultrasound bath presented 7 Lorentzian components with the 2D positions (for the majority of the curves) at 2643–2690 cm^{-1}. This indicates 1–3 layers graphene, which is in agreement with AFM results (Fig. 6c). However, when considering the FWHM this sample presented a value of 82 cm^{-1}, which represents graphene with about 5 layers. Based on this analysis, we assigned this sample as ≤5 layers. Using 117 W ultrasound probe, the exfoliated graphite presented a 2D band deconvolution composed of 8 Lorentzians positioned between 2629 and 2761 cm^{-1}, but with most of them higher than 2700 cm^{-1}. That can be attributed to a less exfoliated material (about 10 layers). When considering also the FWHM value of 81 cm^{-1}, for this sample was assigned between 5 and 10 layers. Finally, using the 280 W ultrasound probe, the exfoliated graphite presented 8 Lorentzian components at the deconvolved 2D band. Most of them were red-shifted from 2700 cm^{-1}, indicating that the LPE process was less effective and produced mostly

Table 2
Comparison between this work and other LPE results in the literature.

Material	Ultrasound type/Power	Centrifugation	Time	I_D/I_G	I_{2D}/I_G	N° layers	Ref
[$(Bnz)_2$Im(Benz)]	Bath/320 W	No	5 h	0.25	1.07	≤5	This work
	Probe/117 W	No	30 min	0.21	0.43	5–10	
	Probe/280 W	No	30 min	0.10	0.33	5-multilayer	
Graphite/NMP	Bath/90 W	500–3000 rpm 45 min	168 h	0.22–0.08	–	1–6	13
Graphite/water DSBS	Bath/90 W	500 rpm 90 min	30 min	–	–	less than5	14
Graphite/NMP	Shear mixer/250 W	1500 rpm 150 min	20 min	0.25–0.35	–	4–7	15

multi-layered platelets (greater than10 layers). As, the FWHM value was 75 cm^{-1}, indicating platelets with less structural disorder [60–61] but with more than 5 layers material (in agreement with AFM, Fig. 6f), for this sample was attributed from 5 layers to multi-layered platelets.

4. Conclusions

Using different experimental techniques (DLS, Raman spectroscopy, AMF, electron microscopy) we showed that graphite LPE to few-layer graphene is feasible using a simple protocol, namely, sonication in emulsion of DCM/W, stabilized by ILs. The efficiency of this mixture is due to the formation of very small droplets at the O/W emulsion. DFT calculations indicated that ILs with aromatic rings in both the cation and anion interact strongly with the formed graphene and presumably inhibit its aggregation. Moreover, the positively charged imidazolium ring exerted an even stronger/tighter binding to the graphene surface than the benzoate and naphthoate anions.

The best condition to produce few-layer graphene was employing below 10% of organic phase (DCM) to the biphasic liquid system, in the presence of [$(Bnz)_2$Im(Benz)], which formed the smallest and most stable organic domains allowing a large interphase area to accommodate the exfoliated graphite. Interestingly, the use of ultrasound bath processor associated with biphasic liquid system proved to be the best way to control the exfoliation efficiency and product quality, although the use of a 117 W ultrasound probe also produced few-layer graphene with good structural quality. The application of a higher power ultrasound probe (280 W) produced a less efficient exfoliation, which seems to be associated to the low boiling point of this specific organic phase (DCM). Comparing these results with other state-of-the-art publications, it was verified that the use of biphasic liquid system containing [$(Bnz)_2$Im(Benz)] allows producing similar results, but with the benefit of avoiding the centrifugation step, once the biphasic liquid system segregates and stabilizes the exfoliated graphite.

The number of studies describing the potential of biphasic liquid systems for LPE is very limited. The results presented herein indicate that a large number of interesting systems can be developed by different solvent pairs, expanding the possibilities for LPE processes.

Acknowledgements

This work has received funding from the European Union's Horizon 2020-MSCA-RISE-734164 Graphene 3D Project, and MackPesquisa (Project number 181009). The authors acknowledge the assistance provided by the Research Infrastructure NanoEnviCz, supported by the Ministry of Education, Youth and Sports of the Czech Republic under Project No. LM2015073, and are also thankful to Ivo Jakubec for performing part of the TEM characterizations. HB, PE and DS acknowledge the Czech Science Foundation (Project 17-08273S) for financial support. LS acknowledge CNPq (Grant 306422/2017-4) for financial support and Centre for Advanced 2D Materials, National University of Singapore (CA2DM/NUS) for high-performance computing facilities. LS, JJP, EATS, RKD (SPEC Project 2012/50259-8) and OAS (project 2014/22136-4) acknowledge FAPESP for financial support. APG is thankful to CAPES for the Ph.D. scholarship. The authors are also thankful to Anton Paar for providing the equipment and support for DSL characterizations.

Appendix A. Supplementary data

Supplementary data to this article can be found online at https://doi.org/10.1016/j.ultsonch.2019.01.016.

References

[1] A.K. Geim, K.S. Novoselov, The rise of graphene, Nat. Mater. 6 (2007) 183–191.
[2] A.K. Geim, Graphene: Status and Prospects, Science 324 (2009) 1530–1534.
[3] K.S. Novoselov, V. Falko, L. Colombo, P.R. Geller, et al., A roadmap for graphene, Nature 490 (2012) 192–200.
[4] A.C. Ferrari, F. Bonaccorso, V. Falko, K.S. Novoselov, S. Roche, et al., Science and technology roadmap for graphene, related two-dimensional crystals, and hybrid systems, Nanoscale 7 (2015) 4598–4810.
[5] L. Shahriary, A.A. Athawale, Graphene oxide synthesized by using modified Hummers approach, Int. J. Renew. Energy Environ. Eng. 2 (2014) 58–63.
[6] H. Mehl, C.F. Matos, E.G.C. Neiva, S.H. Domingues, A.J.G. Zarbin, Efeito da variação de parâmetros reacionais na preparação de grafeno via oxidação e redução do grafite, Quím. Nova 37 (2014) 1639–1645.
[7] A.J.G. Zarbin, M.M. Oliveira, Nanoestruturas de carbono (nanotubos, grafeno): Quo Vadis? Quím. Nova 36 (2013) 1533–1539.
[8] J.N. Coleman, Liquid-phase exfoliation of nanotubes and graphene, Adv. Funct. Mater. 19 (2009) 3680–3695.
[9] C. Backes, T.M. Higgins, A. Kelly, C. Boland, A. Harvey, D. Hanlon, J.N. Coleman, Guidelines for exfoliation, characterization and processing of layered materials produced by liquid exfoliation, Chem. Mater. 29 (2017) 243–255.
[10] V. Štengl, J. Henych, J. Bludská, P. Ecorchard, M. Kormunda, A green method of graphene preparation in an alkaline environment, Ultrason. Sonochem. 24 (2015) 65–71.
[11] R.G. Bai, K. Muthoosamy, F.N. Shipton, A. Pandikumar, P. Rameshkumar, N.M. Huang, S. Manickam, Biogenic synthesis of reduced graphene oxide-silver (rGO-Ag) nanocomposite and its dual applications as antibacterial agent and cancer biomarker sensor, RSC Adv. 6 (2016) 36576–36587.
[12] J. Zhang, H. Yang, G. Shen, P. Cheng, J. Zhang, S. Guo, Reduction of graphene oxide via L-ascorbic acid, Chem. Commun. 46 (2010) 1112–1114.
[13] Y. Wang, Z. Shi, J. Yin, Facile synthesis of soluble graphene via a green reduction of graphene oxide in tea solution and its biocomposites, ACS Appl. Mater. Interf. 3 (2011) 1127–1133.
[14] E.C. Salas, Z. Sun, A. Lüttge, J.M. Tour, Reduction of graphene oxide via bacterial respiration, ACS Nano. 4 (2010) 4852–4856.
[15] K. Muthoosamy, S. Manickam, State of the art and recent advances in the ultrasound-assisted synthesis, exfoliation and functionalization of graphene derivatives, Ultrason. Sonochem. 39 (2017) 478–493.
[16] K.R. Paton, et al., Scalable production of large quantities of defect-free few layers graphene by shear exfoliation in liquids, Nat. Mater. 13 (2014) 624–630.
[17] A.B. Bourlinos, V. Georgakilas, R. Zboril, T.A. Steriotis, A.K. Stubos, Liquid-phase exfoliation of graphite towards solubilized graphene, Small 5 (2009) 1841–1845.
[18] U. Khan, A. O'Neill, H. Porwal, P. May, et al., Size selection of dispersed, exfoliated graphene flakes by controlled centrifugation, Carbon 50 (2012) 470–475.
[19] Y. Hernandez, V. Nicolosi, M. Lotya, F.M. Blighe, Z. Sun, et al., High-yield production of graphene by liquid-phase exfoliation of graphite, Nat. Nanotechnol. 3 (2008) 563–568.
[20] J.N. Coleman, Liquid exfoliation of defect-free graphene, Acc. Chem. Res. 46 (2013) 14–22.
[21] V. Georgakilas, J.N.K. Tiwari, C. Kemp, J.A. Perman, A.B. Bourlinos, K.S. Kim, R. Zboril, Noncovalent functionalization of graphene and Graphene Oxide for energy materials, Biosensing, Catalytic, and Biomedical Applications, Chem. Rev. 116 (2016) 5464–5519.
[22] V. Georgakilas, M. Otyepka, A.B. Bourlinos, V. Chandra, N. Kim, K.C. Kemp, P. Hobza, R. Zboril, K.S. Kim, Functionalization of graphene: covalent and non-covalent approaches, Derivatives and Applications, Chem. Rev. 112 (2012) 6156–6214.
[23] M. Buzaglo, I.P. Bar, M. Varenik, L. Shunak, S. Pevzner, O. Regev, Graphite-to-graphene: total conversion, Adv. Mater. 29 (2017) 1603528.
[24] K.Z. Donato, L. Matějka, R.S. Mauler, R.K. Donato, Recent Applications of Ionic Liquids in the Sol-Gel Process for Polymer-Silica Nanocomposites with Ionic Interfaces, Colloids Interf. 1 (2017) 5.
[25] M. Perchacz, R.K. Donato, L. Seixas, A. Zhigunov, R. Konefał, M. Serkis-Rodzeń, H. Beneš, Ionic Liquid-Silica Precursors via Solvent-Free Sol-Gel Process and Their Application in Epoxy-Amine Network: A Theoretical/Experimental Study, ACS Appl. Mater. Interf. 9 (2017) 16474–16487.
[26] J. Dupont, On the solid, liquid and solution structural organization of imidazolium ionic liquids, J. Braz. Chem. Soc. 15 (2004) 341–350.
[27] J. Eastoe, S. Gold, S.E. Rogers, A. Paul, T. Welton, R.K. Heenan, I. Grillo, Ionic liquid-in-oil microemulsions, J. Am. Chem. Soc. 127 (2005) 7302–7303.
[28] J.P. Hallett, T. Welton, Room-temperature ionic liquids: solvents for synthesis and catalysis 2, Chem. Rev. 111 (2011) 3508–3576.
[29] K.Z. Donato, M. Lavorgna, R.K. Donato, M.G. Raucci, G.G. Buonocore, L. Ambrosio, H.S. Schrekker, R.S. Mauler, High amorphous vinyl alcohol-silica bionanocomposites: tuning interface interactions with ionic liquids, ACS Sustain. Chem. Eng. 5 (2017) 1094–1105.
[30] V. Chaban, E.E. Fileti, Graphene exfoliation in ionic liquids: unified methodology, RSC Adv. 5 (2015) 81229–81234.
[31] X. Wang, P.F. Fulvio, G.A. Baker, G.M. Veith, R.R. Unocic, S.M. Mahurin, M. Chib, S. Dai, Direct exfoliation of natural graphite into micrometer size few layers graphene sheets using ionic liquids, Chem. Commun. 46 (2010) 4487–4489.
[32] D. Nuvoli, L. Valentini, V. Alzari, S. Scognamillo, S. Bittolo Bon, M. Piccinini, J. Illescasd, A. Mariani, High concentration few-layer graphene sheets obtained by liquid phase exfoliation of graphite in ionic liquid, J. Mater. 21 (2011) 3428–3431.
[33] N.G. Shang, P. Papakonstantinou, S. Sharma, G. Lubarsky, G. Lubarsky, M. Li, D.W. McNeill, A.J. Quinn, W. Zhoue, R. Blackleye, Controllable selective exfoliation of high-quality graphene nanosheets and nanodots by ionic liquids assisted grinding, Chem. Commun. 48 (2012) 1877–1879.
[34] M. Matsumoto, Y. Saito, C. Park, T. Fukushima, T. Aida, Ultrahigh-throughput exfoliation of graphite into pristine 'single-layer' graphene using microwaves and

molecularly engineered ionic liquids, Nat. Chem. 7 (2015) 730–736.
[35] R. Bari, G. Tamas, I. Fahmida, A.J.A. Aquino, M.J. Greena, E.L. Quitevis, Direct exfoliation of graphene in ionic liquids with aromatic groups, Colloids Surf. A Physicochem. Eng. Asp. 463 (2014) 63–69.
[36] K.S. Suslick, Y. Didenko, M.M. Fang, T. Hyeon, K.J. Kolbeck, W.B. McNamara III, M.M. Mdleleni, M. Wong, Acoustic cavitation and its chemical consequences, Phil. Trans. R. Soc. Lond. A. 357 (1999) 335–353.
[37] Y. Wei, Z. Sun, Liquid-phase exfoliation of graphite for mass production of pristine few-layer graphene, Curr. Opin. Colloid Interf. Sci. 20 (2015) 311–321.
[38] G. Cravotto, P. Cintas, Sonication-assisted fabrication and post-synthetic modifications of graphene-like materials, Chem. Eur. J. 16 (2010) 5246–5259.
[39] D. Radziuk, H. Möhwald, Ultrasonically treated liquid interfaces for progress in cleaning and separation processes, Phys. Chem. Chem. Phys. 18 (2016) 21–46.
[40] B. Abismaïl, J.P. Canselier, A.M. Wilhelm, H.C. Delmas, C. Gourdon, Emulsification by ultrasound: drop size distribution and stability, Ultrason. Sonochem. 6 (1999) 75–83.
[41] J.P. Canselier, H. Delmas, A.M. Wilhelm, B. Abismaïl, Ultrasound Emulsification - an overview, J. Dispers. Sci. Technol. 23 (2002) 333–349.
[42] M. Tariq, M.G. Freire, B. Saramago, J.A.P. Coutinho, J.N. Canongia- Lopes, L.P.N. Rebelo, Surface tension of ionic liquids and ionic liquid solutions, Chem. Soc. Rev. 41 (2012) 829–868.
[43] M. Sivakumar, S.Y. Tang, K.W. Tan, Cavitation technology - a greener processing technique for the generation of pharmaceutical nanoemulsions, Ultrason. Sonochem. 21 (6) (2014) 2069–2083.
[44] H. Beneš, R.K. Donato, P. Ecorchard, D. Popelková, E. Pavlová, D. Schelonka, O. Pop-Georgievski, H.S. Schrekker, V. Štengl, Direct delamination of graphite ore into defect-free graphene using a biphasic solvent sytem under pressurized ultrasound, RSC Adv. 6 (2016) 6008–6915.
[45] W.L.F. Armarego, D.D. Perrin, Purification of Laboratory Chemicals, 4th ed., Butterworth-Heinemann, Oxford, U.K., 1997.
[46] C. James, C. Ravikumar, V.S. Jayakumar, I. Hubert, Vibrational spectra and potential energy distributions for 1-benzyl-1H-imidazole by normal coordinate analysis, J. Raman Spectrosc. 40 (2008) 537.
[47] W. Kohn, L.J. Shan, Self- consistent equations including exchange and correlation effects, Phys. Rev. 140 (1965) A1133–A1138.
[48] J.M. Soler, E. Artacho, J.D. Gale, A. García, J. Junquera, P. Ordejón, D. Sánchez-Portal, The SIESTA method for ab initio order-n materials simulation, J. Phys. Condens. Matter. 14 (2002) 2745–2779.
[49] J.P. Perdew, K. Burke, M. Ernzerhof, Generalized Gradient Approximation made simple, Phys. Rev. Lett. 77 (1996) 3865–3868.
[50] N. Troullier, J.L. Martins, Efficient pseudopotentials for plane-wave calculations, Phys. Rev. B Condens. Matter Mater. Phys. 43 (1991) 1993–2006.
[51] H.J. Monkhorst, J.D. Pack, Special points for Brillouin-zone integrations, Phys. Rev. B: Condens. Matter Mater. Phys. 13 (1976) 5188–5192.
[52] S. Grimme, Semi Empirical GGA-Type Density Functional constructed with a long-range dispersion correction, J. Comp. Chem. 27 (2006) 1787–1799.
[53] N. Bowden, F. Arias, T. Deng, G.M. Whitesides, Self-assembly of microscale objects at a liquid/ liquid interface through lateral capillary forces, Langmuir 17 (2001) 1757–1765.
[54] W.H. Binder, Supramolecular assembly of nanoparticles at liquid–liquid interfaces, Angew. Chem. Int. Ed. 44 (2005) 5172–5175.
[55] S. Biswas, L.T. Drzal, A novel approach to create a highly ordered monolayer film of graphene nanosheets at the liquid-liquid interface, Nano Lett. 9 (2009) 167–172.
[56] D. Wang, H. Duan, H. Möhwald, The water/ oil interface: the emerging horizon for self-assembly of nanoparticles, Soft Matter 1 (2005) 412–416.
[57] S.J. Woltornist, A.J. Oyer, J.M. Carrillo, Y.A.V. Dobrynin, D.H. Adamson, Conductive thin films of pristine graphene by solvent interface trapping, ACS Nano 7 (2013) 7062–7066.
[58] A.C. Ferrari, J.C. Meyer, V. Scardaci, C. Casiraghi, M. Lazzeri, F. Mauri, S. Piscanec, Da Jiang, K.S. Novoselov, S. Roth, A.K. Geim, The Raman fingerprint of graphene, Phys. Rev. Lett. 97 (2006) 187401–187406.
[59] A.C. Ferrari, D. Basko, Raman Spectroscopy as a versatile tool for studying the properties of graphene, Nat. Nanotech. 8 (2013) 235–246.
[60] L.G. Cançado, A. Jorio, E.H. Martins Ferreira, F. Stavale, C.A. Achete, R.B. Capaz, M.V.O. Moutinho, A. Lombardo, T.S. Kulmala, A.C. Ferrari, Quantifying Defects in graphene via Raman Spectroscopy at different excitation energies, Nano Lett. 11 (2011) 3190–3196.
[61] Y. Hao, Y. Wang, L. Wang, Z. Ni, et al., Probing layer number and stacking order few-layer graphene by Raman Spectroscopy, Small 6 (2010) 195–200.